

Proper motions with Subaru II. A sample in the Subaru/XMM-Newton Deep Survey field *

Michael W. RICHMOND

*Physics Department, Rochester Institute of Technology,
Rochester, NY 14623, USA
mwrsp@rit.edu*

Tomoki MOROKUMA

*Research Fellow of the Japan Society for the Promotion of Science,
Optical and Infrared Astronomy Division, National Astronomical Observatory of Japan,
2-21-1 Osawa, Mitaka, Tokyo 181-8588, Japan
tomoki.morokuma@nao.ac.jp*

Mamoru DOI

*Institute of Astronomy, Graduate School of Science, University of Tokyo,
2-21-1, Osawa, Mitaka, Tokyo 181-0015, Japan
doi@ioa.s.u-tokyo.ac.jp*

Yutaka KOMIYAMA

*Optical and Infrared Astronomy Division, National Astronomical Observatory of Japan,
2-21-1 Osawa, Mitaka, Tokyo 181-8588, Japan
komiyama@subaru.naoj.org*

Naoki YASUDA

*Institute for the Physics and Mathematics of the Universe, University of Tokyo,
5-1-5 Kashiwa-no-ha, Kashiwa, Chiba 277-8568, Japan
yasuda@icrr.u-tokyo.ac.jp*

and

Sadanori OKAMURA

*Department of Astronomy and Research Center for the Early Universe, School of Science, University of Tokyo
7-3-1 Hongo, Bunkyo, Tokyo 113-0033, Japan
okamura@astron.s.u-tokyo.ac.jp*

(Received ; accepted)

Abstract

We search for stars with proper motions in a set of deep Subaru images, covering about 0.48 square degrees to a depth of $i' \simeq 26$, taken over a span of five and a half years. We follow the methods described in Richmond et al. (2009) to reduce and analyze this dataset. We present a sample of 69 stars with motions of high significance, and discuss briefly the populations from which they are likely drawn. Based on photometry and motions alone, we expect that 14 of the candidates may be white dwarfs. Our candidate with the largest proper motion is surprisingly faint and likely to prove interesting: its colors and motions suggest that it might be an M dwarf moving at over 500 km/sec or an L dwarf in the halo.

Key words: stars: kinematics — Galaxy: kinematics and dynamics — Galaxy: structure

1. Introduction

This paper continues our effort to use the Subaru telescope to search for proper motions among very faint stars. Our first paper (Richmond et al. 2009) examined a series of images of the Subaru Deep Field (SDF) (Kashikawa et al. 2004), located close to the Northern Galactic Pole ($l = 37^\circ 6$, $b = +82^\circ 6$). We report here on a similar analysis of images of the Subaru/XMM-Newton Deep Survey (SXDS) field (Sekiguchi et al. 2005, Furusawa et al. 2008, Morokuma et al. 2008), which lies at high galactic latitude in the southern galactic

hemisphere ($l \simeq 170^\circ$, $b \simeq -60^\circ$). As in our earlier work, we are taking advantage of a dataset compiled for the study of very distant extragalactic objects; the long time coverage necessary to detect supernovae and AGN provides us with the baseline needed to measure proper motions for a significant number of stars in our own Milky Way. We pay special attention to members of the faintest stellar populations, white dwarfs.

Since we will follow very closely the methods used in our analysis of the SDF, we urge the reader to consult Richmond et al. (2009) for a detailed description of some procedures we may mention only briefly here. However, the SXDS dataset differs from the SDF dataset in one very important way: it consists of a mixture of images taken through two passbands, the Suprime-Cam R_c and i' (Miyazaki et al. 2002), while the SDF

* Based in part on data collected at the Subaru Telescope, which is operated by the National Astronomical Observatory of Japan.

data was all taken through i' . This inhomogeneity complicates efforts to determine the selection effects which define our sample of moving objects; therefore, we discuss in depth our tests of the magnitudes and motions to which our analysis of the SXDS is reasonably complete. One of our goals in this project is to compare observed sets of moving stars to those predicted by various models of stellar populations in the Milky Way. We will need a good understanding of the selection effects on the observations in order to compare them fairly to models in a future paper.

Section 2 describes the observations and the steps we took to convert the raw images into clean, seamless mosaic images. We list in section 3 our procedures for finding and measuring the properties of stars in the images, yielding a list of formal motions for tens of thousands of stars. Most of these motions, of course, were not significantly different from zero, and so we discuss in section 4 our techniques for selecting a small subset of stars with significant proper motions. We used artificial stars inserted into our images to estimate the completeness of our sample as a function of magnitude and motion, and, to a limited degree, color. In section 5, we briefly compare our sample of moving stars with those found in the SDF and predicted in the the Besançon model (Robin et al. 2003). We also highlight one very interesting star, which combines a large proper motion with a very faint apparent magnitude.

2. Observations

The Subaru/XMM-Newton Deep Survey (SXDS) involves sensitive measurements across a wide range of wavelengths over a region of about 1.3 square degrees (Sekiguchi et al. 2005, Furusawa et al. 2008). Since the main goal of the project is to study extragalactic objects, the field is located at relatively high galactic latitude ($b = -60^\circ$). We analyze a subset of the optical images taken with the Subaru 8.2-meter telescope and Suprime-Cam camera (Miyazaki et al. 2002). The regions in the southern (SXDS-S) and eastern (SXDS-E) sections of the survey (see Figure 1 and Table 1) were observed at least 11 times over the period September, 2002, to January, 2008. We provide a list of the observations in Table 2. Note that data taken on September 29 and September 30, 2002, were combined to form a single composite image.

We followed the procedure described in Richmond et al. (2009) to reduce the raw images and combine them to form a single seamless mosaic for each night. The FWHM of the mosaics varied from $0''.59$ on the best night to $1''.11$ on the worst, but since the plate scale was $0''.202$ per pixel, all images were adequately sampled.

The limiting magnitude varied slightly, but on average was about $i' \sim 26.0$ (see Section 3). These measurements reach about 0.5 magnitudes deeper than those reported in Richmond et al. (2009); combined with the larger sky coverage, this study encompasses a larger volume. We estimate the effective volume for stars of absolute magnitude $M_V = +16.5$ to be 130000 cubic parsecs, about four times as large as that of Richmond et al. (2009) (the value of 14000 cubic parsecs shown in Table 1 of that paper was an error; the proper value is 28000 cubic parsecs).



Fig. 1. Subregions within the SXDS in which we measured proper motions. North is up, East to the right. The entire field is about 1.3 degrees on a side.

3. Searching for moving objects

We now describe briefly the steps we took to reduce the clean mosaic images into a list of starlike objects, and then to find objects with significant motions. The reader can find a detailed description of our methods in Richmond et al. (2009).

Our first step was to identify and measure the properties of starlike objects. We used the “stars” program in the *XVista* package (Treffers & Richmond 1989)¹ to find objects with $0''.6 < \text{FWHM} < 1''.4$. The images taken on September 22, 2003, contained the largest number of objects: 79000 in SXDS-E and 86000 in SXDS-S. We therefore made this the fiducial epoch for matching and astrometry. We broke each image into overlapping subsections roughly $200''$ on a side and used the *match* package (Droege et al. 2006)² to transform the subsections in each image to the fiducial’s coordinate system. We looked for matches between epochs using a maximum separation of $1''.0$ from the fiducial position of each star. This places an upper limit of about $0''.23$ per year on the proper motions we could detect, but, as we will show later, this does not have a strong effect on the results.

In order to test the completeness of our object detection, we used a set of artificial stars inserted into the images of SXDS-S. Because this field was observed one fewer time than SXDS-E, the limits we derive from it will likely be conservative estimates for SXDS-E. The tests are complicated by the mixture of passbands in the dataset: eight in i' and three in R_c , including the critical final image taken in 2008. We therefore ran three sets of tests, using artificial stars with colors ($R_c - i'$) of 0.0, 1.0 and 2.0 magnitudes. For each color, we created 1000 artificial stars and inserted them at locations known to be free

¹ <http://spiff.rit.edu/tass/xvista>

² <http://spiff.rit.edu/match>

Table 1. Regions in the SXDS (equinox J2000)

Name	min RA	max RA	min Dec	max Dec
SXDS-E	02:18:55	02:20:34	-05:17:24	-04:43:12
SXDS-S	02:16:37	02:18:54	-05:32:22	-05:06:50

Table 2. Observations of the SXDS

UT Date	Julian Date - 2,450,000	Filter	Exptime (seconds)
SXDS-E			
2002 Sep 29, 30	2548.5	i'	3000
2002 Nov 1	2579.9	i'	3000
2002 Nov 1	2580.0	R_c	1500
2002 Nov 2	2580.8	i'	1800
2002 Nov 9	2587.8	i'	2820
2002 Nov 9	2588.0	R_c	210
2002 Nov 29	2608.0	i'	1800
2003 Sep 22	2905.0	i'	6000
2003 Oct 2	2915.1	i'	1271
2003 Oct 21	2934.1	i'	1400
2005 Sep 28	3642.0	i'	3600
2008 Jan 9	4474.8	R_c	2400
SXDS-S			
2002 Sep 29, 30	2548.4	i'	3000
2002 Nov 1	2579.9	i'	3600
2002 Nov 1	2580.0	R_c	2400
2002 Nov 2	2580.8	i'	1800
2002 Nov 9	2587.8	i'	2580
2002 Nov 9	2588.0	R_c	2400
2002 Nov 29	2608.0	i'	1500
2003 Sep 22	2905.0	i'	4500
2003 Oct 2	2915.1	i'	2040
2005 Sep 28	3642.0	i'	2040
2008 Jan 9	4474.7	R_c	2400

of real stars in each image. We then executed our procedures to find and match stars. We required stars to appear in at least five epochs to qualify for further study. Figure 2 indicates that the fraction of artificial stars entering our proper motion study dropped to 50% at $i' \simeq 26.0$ regardless of color.

A large number of objects qualified for the next step by appearing in at least five images: 47589 in SXDS-S and 45500 in SXDS-E. We considered the row and column positions of each object separately, making a linear fit to each as a function of time. As described in Richmond et al. (2009), we derived the one-dimensional motion in rows and columns, as well as the uncertainty in each motion. Figure 3 indicates that the precision of our measurements of position in the SXDS is roughly the same as that of our measurements in the SDF. The median deviation in each direction from the fitted motion ranged from $0''.01$ for bright unsaturated stars to $0''.05$ for the faintest objects in our sample.

4. Choosing objects with significant motions

We defined statistics S_{row} and S_{col} as the ratios of motion to uncertainty in each direction, and computed the overall sig-

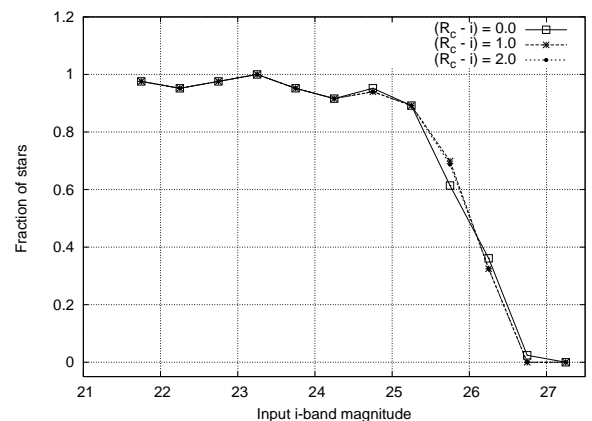


Fig. 2. Fraction of artificial stars added to the images which were detected and matched in at least 5 epochs.

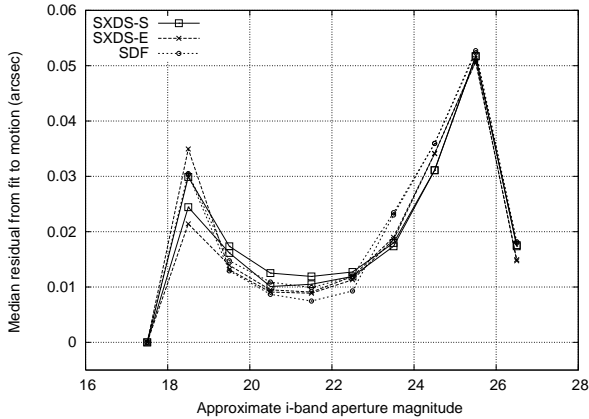


Fig. 3. Comparison of residuals from fitted proper motions along rows and along columns in the SDF and SXDS.

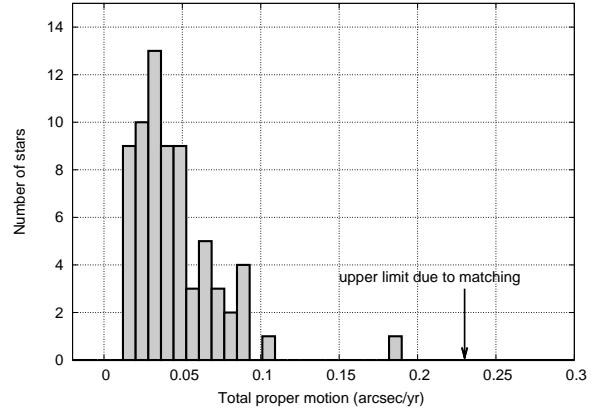


Fig. 5. Distribution of detected proper motions.

nificance of each object’s motion as $S_{\text{tot}} \equiv \sqrt{S_{\text{row}}^2 + S_{\text{col}}^2}$. We chose a conservative threshold, $S_{\text{tot}} \geq 5$, to create samples of “candidates for stars with proper motions.” Only a small number of objects entered these samples: 40 in the SXDS-S and 33 in the SXDS-E. The fraction of all objects having significant motions was only about 0.7%, smaller than the 1.4% found in the SDF. Since the uncertainties in individual measurements were roughly the same in both areas, but stars were measured almost twice as frequently in the SDF, a fixed value of S_{tot} corresponds to a smaller absolute motion in the SDF than in the SXDS fields.

The time sampling of our survey was far from uniform, and there was a three-year gap between the penultimate and final measurement. Moreover, that final measurement was made through the R_c filter, rather than the i' filter used for most of the images. Since that final image influences the proper motions strongly, it is possible that there might be some color dependency in our proper motion sample. Therefore, we ran a set of tests using three sets of artificial stars: one group had colors $(R_c - i') = 0$, one $(R_c - i') = 1$, and one $(R_c - i') = 2$. We generated 1000 stars in each group with i' -band magnitudes $21 \leq i' \leq 25$ and proper motions $0.0 \leq \mu \leq 0.10$ per year in random directions. We inserted these artificial stars into our images, analyzed them as described above, and counted the number which appeared in our output set of stars detected as moving with significance $S_{\text{tot}} \geq 5$. As Figure 4 shows, the efficiency with which we detect moving stars does depend on color for the faintest stars: we recover faint blue stars at a higher rate than faint red stars. At the bright end, our efficiency drops to 50% for motions less than about 0.04 per year for stars of all colors. Our search in the SXDS is slightly less sensitive to stars with small motions than our search in the SDF, due to the smaller number of images over a similar span of time.

We show in Figure 5 the distribution of measured proper motions. The upper limit of 0.23 per year is set by the matching limit of 1.0 and the time difference between our fiducial epoch (Sept 22, 2003) and the final epoch (Jan 9, 2008). Since all but a single object have motions less than half this value, we conclude that the limit set by our matching procedures does not bias our final results. We will discuss the one object with

$\mu \sim 0.18$ per year in the next section.

We examined each candidate visually at several epochs to verify that the motions were real. We found 1 object in the SXDS-S and 3 in the SXDS-E which had bogus motions due to blends of two stars or a star and a galaxy. Discarding those left 39 candidates in the SXDS-S and 30 candidates in the SXDS-E.

We extracted corrected isophotal magnitudes in B , V , R_c and i' passbands for each candidate from the catalogs of Furusawa et al. 2008 and compared them to the visual appearance of the candidate in images taken from the SXDS Data Release 1³. In several cases (5 in SXDS-S, 4 in SXDS-E), we noticed an obvious discrepancy, always in the same sense: the catalog magnitude indicated a much brighter object than actually appeared in the images. We suspect that the matching procedure used to create the catalogs may have confused neighboring objects with very different colors. Therefore, we corrected the magnitudes of these candidates as follows: we measured instrumental magnitudes of all candidates in the B , V , R_c and i' images of the SXDS Data Release 1 using a small aperture, 1 arcsecond in radius. We examined the difference between our instrumental magnitudes and the catalog magnitudes in each passband; in all cases, we found a nearly constant offset for both bright and faint stars, except for a few outliers. We then applied this offset to the instrumental magnitudes of the outliers. The discrepancies were largest in the B and V passbands and almost zero in i' .

There is a small region of overlap between the SXDS-S and SXDS-E, as one can see in Figure 1. We noticed that two of the candidates in this region were actually the same object, detected and measured independently in each set of images. This object was one of the photometric outliers and serves as a test of our ability to compute accurate magnitudes. The difference in corrected magnitudes was 0.03, 0.04 and 0.08 mag in V , R_c and i' , respectively. The annual proper motions derived in each set of images agreed very well: 0.049 ± 0.006 versus 0.052 ± 0.006 in RA, and -0.011 ± 0.004 versus -0.008 ± 0.008 in Dec. However, when we compared the positions for this object drawn separately from the SXDS-E and SXDS-S catalogs of Furusawa et al. (2008), we found differ-

³ <http://step.mtk.nao.ac.jp/sxds/>

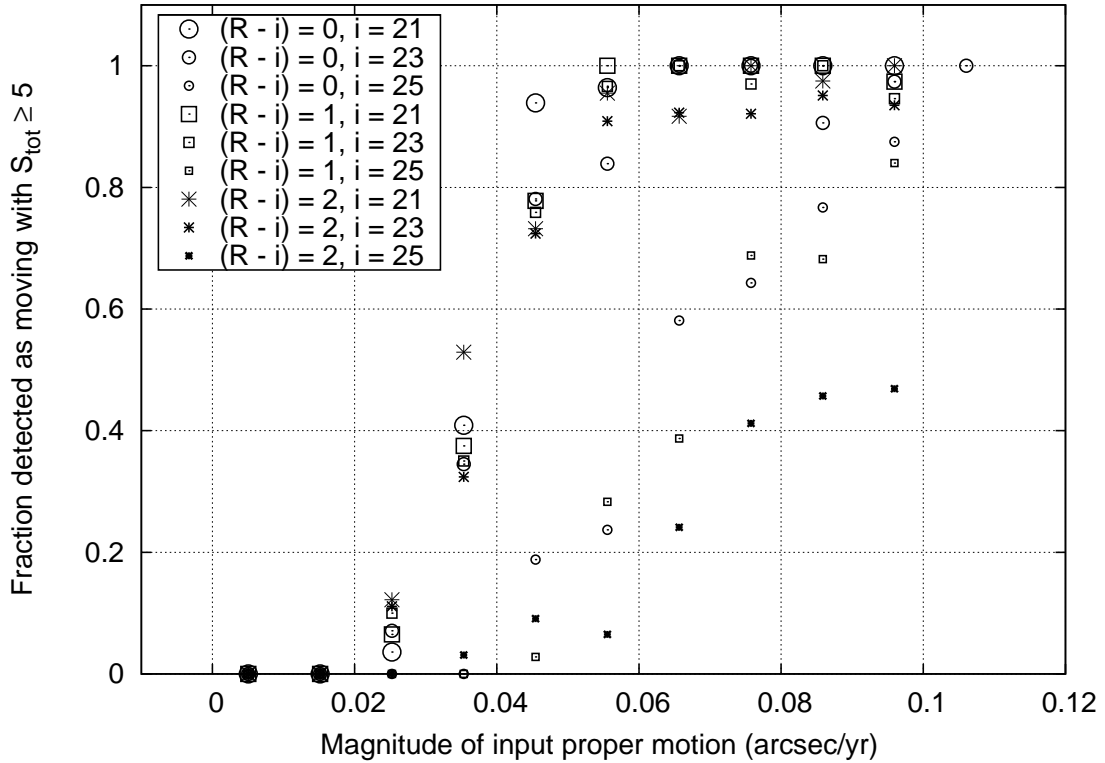


Fig. 4. Results of tests using moving artificial stars to check completeness as a function of color and motion.

ences of $0''.50$ in RA and $0''.25$ in Dec. This may indicate the accuracy of the positions of the objects shown in Table 3.

The result is a sample of 68 stars with significant proper motions and good photometry in four passbands. We list these stars in Table 3. As a final check on the reality of the motions, we can compare the measured motions to those predicted by the Besançon model of stellar populations within the Milky Way Galaxy. Figure 6 shows that our measured motions are predominantly in the southeastern direction, agreeing with the model.

5. Discussion

Following Richmond et al. (2009), we computed the reduced proper motion for the candidates in our sample in order to separate stars belonging to different populations. Figure 7 compares stars in our sample to stars in a simulation of the region based on the Besançon model. The regions drawn in the diagram are exactly the same as those shown in Figures 7 and 8 of Richmond et al. (2009). We adopt their relationship

$$(V - I) = 0.391 + 1.1145(V_s - i') \quad (1)$$

to compare our results to the models.

Of the 68 objects in our sample, 13 lie within the “white dwarf” (WD) region of the diagram, 32 within the “halo” region, 12 within the “disk” region, 10 within the “halo sd?” region, and 1 falls far from all the rest (we discuss that outlier below). The fraction of stars in each region agree reasonably well with the fractions found in our survey of the SDF. Although the

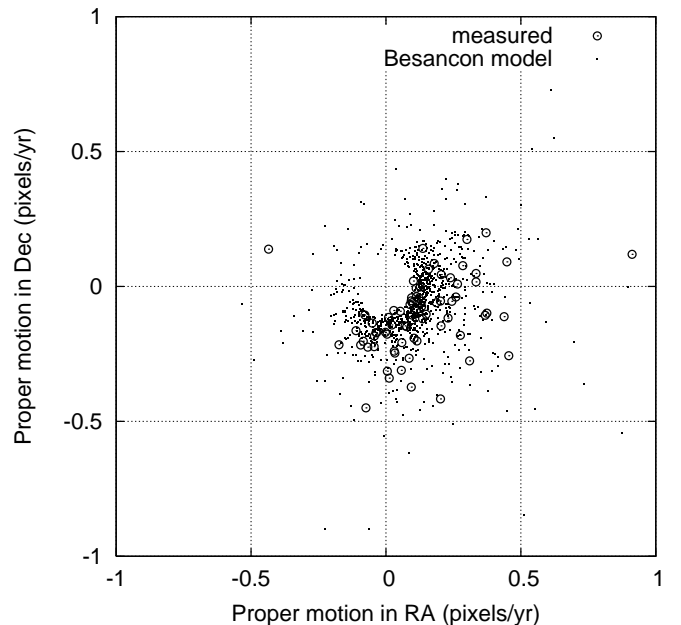


Fig. 6. Comparison of measured and model proper motions for stars in the SXDS.

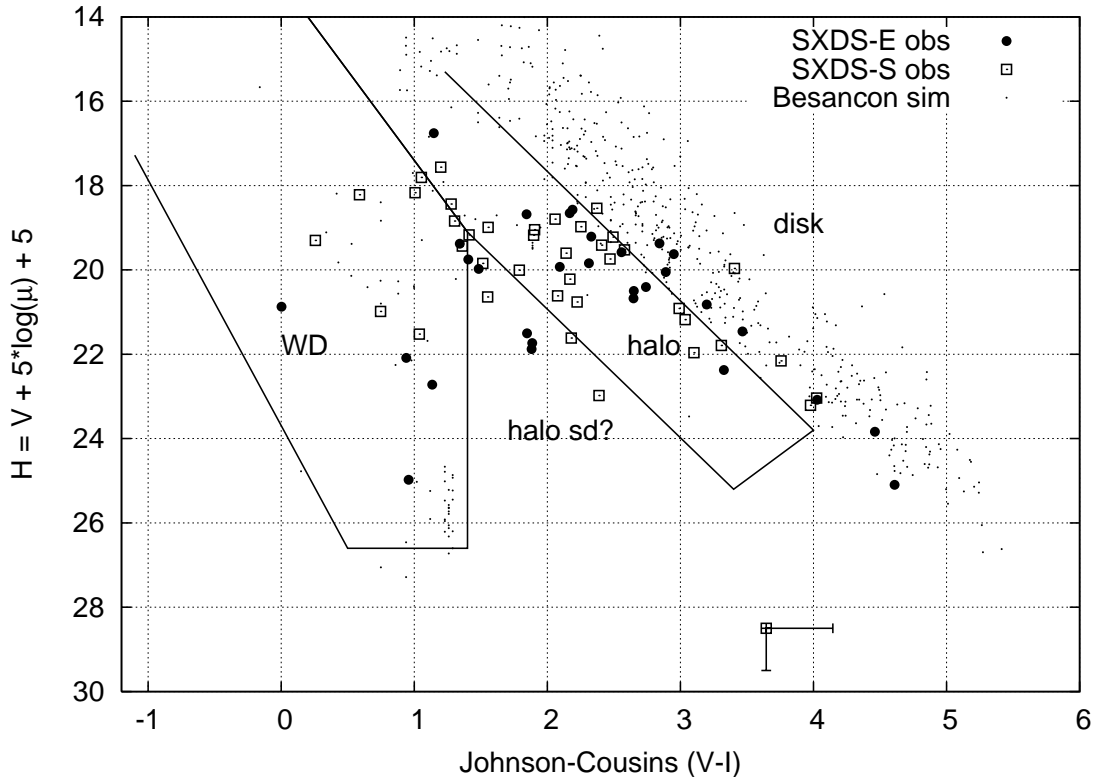


Fig. 7. Reduced proper motion diagram for observed objects in the SXDS and simulated objects based on the Besançon model. Real objects have errorbars in both directions, though some are too small to see. The object at lower right is placed according to lower limits to its V -band magnitude; see text for details.

fraction of objects in the WD region (19%) is somewhat higher than in the SDF (9%), we do not consider the difference significant, given the small number of objects in each set, and the number of objects lying very close to the somewhat arbitrary boundaries of the WD region in each sample.

We performed multiple simulations using the Besançon model to generate stars in the SXDS over an effective area of two square degrees. We applied the selection criteria derived in Section 3 to these simulated catalogs, then scaled the results to the actual area we observed (0.48 square degrees). We found a total of 12.5 WD in the simulation, which agrees well with the 13 candidates in the WD region of our reduced proper motion diagram. Over half (56%) of the WDs in the simulation were members of the halo, with most of the remainder (34%) drawn from the thick disk.

One of the candidates, SXDSPM J021840.0-053623, deserves individual attention. It has the highest proper motion in our sample, $0''.186$ per year (see Figures 8 and 9), and yet is very faint: $R_c = 26.09$, $i' = 24.38$, $z = 22.62$. The object is very red: our attempt to measure a magnitude at the object's position in the V_s -band image yielded a formal value of $V_s \sim 28.3$, but we choose instead to quote a lower limit of $V_s \geq 27.3$ based on secure measurements of faint stars nearby. Its colors ($R_c - i' = 1.69$ and $i' - z = 1.76$) place it far from the locus of cool main sequence stars. If we use the more reliable ($i' - z$) color alone, the star might be an M9 dwarf (Hawley et al. 2002, West et al. 2005) with an absolute mag-

nitude $M_i \simeq 15.5 \pm 0.5$. However, in that case, the distance to the object would be $\sim 600 \pm 120$ pc, and the tangential velocity $v_t \sim 520 \pm 180$ km/s. The $(i' - z)$ color of an L2 dwarf is not very different from our value, and the absolute magnitude of such a star, $M_i \simeq 17.0 \pm 0.5$, would yield a lower velocity, $v_t \sim 260 \pm 90$ km/s, consistent with the halo population. The residuals from a simple linear fit to the object's motion show no sign of parallax, which indicates that it must be at least ~ 20 pc away from the Sun.

The proper motions computed in this paper complement those we described in Richmond et al. (2009), since the SXDS lies in the southern galactic hemisphere and the SDF in the northern. Together, they comprise a set of 167 stars with reliable motions and multicolor photometry. We have characterized the selection effects of both samples as a function of magnitude, proper motion, and (for the SXDS) color. Our next step will be to compare rigorously the properties of the stars in our samples with the predictions made by current models of galactic populations, paying special attention to the objects likely to be white dwarfs.

We thank the staff at the Subaru Telescope for their assistance with the observations used in this project. MWR gratefully acknowledges grant S-03031 from the JSPS Invitation Fellowship for Research in Japan. TM is financially supported by the Japan Society for the Promotion of Science (JSPS) through the JSPS Research Fellowship. Data analysis was in part carried out on the common use data analysis computer

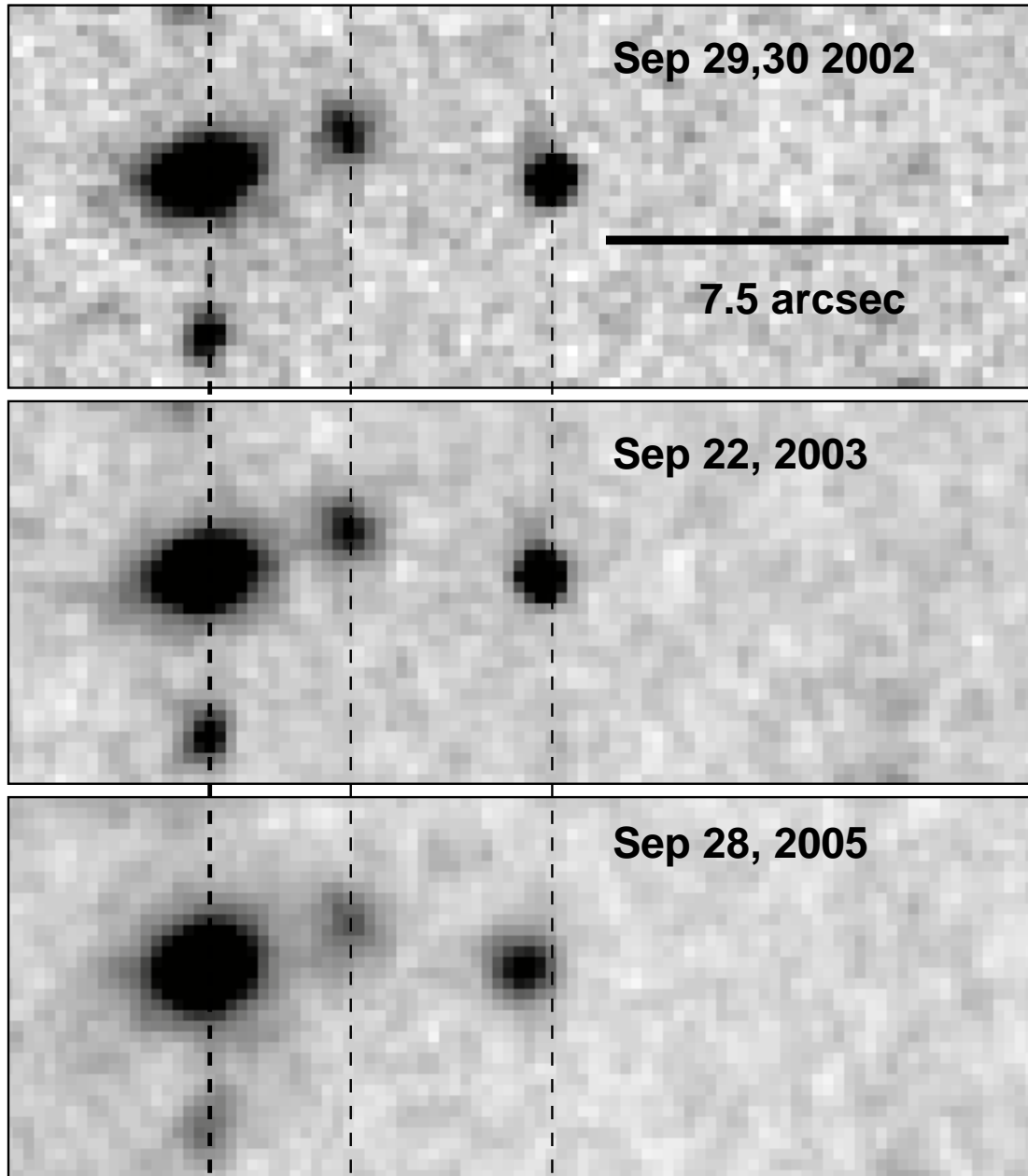


Fig. 9. Images of SXDSPM J021840.0-053623 (at center) in i' -band over a three-year period. North is up and East to the left. Vertical lines have been drawn through the centers of objects in the 2002 image to show relative east-west motion clearly.

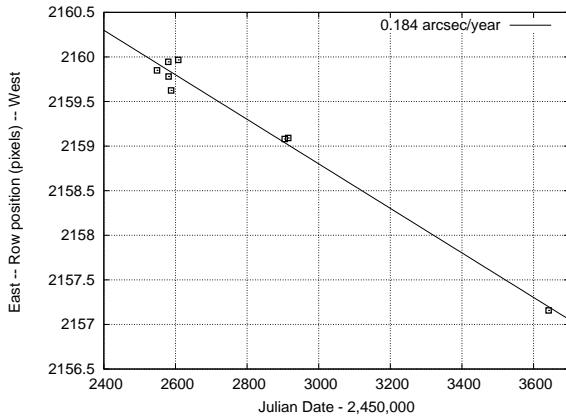


Fig. 8. Motion of SXDSPM J021840.0-053623 in Right Ascension over the period Sep 29, 2002 to Sep 28, 2005. We could not determine a precise position of the object in the R_c -band image of Jan 9, 2008.

system at the Astronomy Data Center, ADC, of the National Astronomical Observatory of Japan.

References

- Droege, T. F. et al. 2006, *PASP*, 118, 1666
 Furusawa, H. et al. 2008, *ApJS*, 176, 1
 Hawley, S. L. et al. 2002, *AJ*, 123, 3409
 Kashikawa, N. et al. 2004, *PASJ*, 56, 1011
 Miyazaki, S. et al. 2002, *PASJ*, 54, 833
 Morokuma, T. et al. 2008, *ApJ*, 676, 163
 Robin, A. C., Reyl , C., Derri re, S., & Picaud, S. 2003, *A&A*, 409, 523
 Richmond, M. W. et al. 2009, *PASJ*, 61, 1
 Sekiguchi, K. et al. 2005, in *Multiwavelength mapping of galaxy formation and evolution (Proceedings of the ESO Workshop held at Venice, Italy)*, ed. A. Renzini & R. Bender (Berlin: Springer-Verlag), 82
 Treffers, R. R. & Richmond, M. W. 1989, *PASP*, 101, 725
 West, A. A., Walkowicz, L. M., & Hawley, S. L. 2002, *PASP*, 117, 706

Table 3. First sample of proper motion candidates in the SXDS

ID	RA*	Dec*	V^{**}	R_c^{**}	i'^{**}	z'^{**}	RA PM [†]	Dec PM [†]
SXDSPM J021651.8-053629	34.21609	-5.60829	20.099	19.287	18.322	17.401	0.048 ± 0.006	0.006 ± 0.006
SXDSPM J021658.4-051453	34.24373	-5.24807	20.309	20.143	20.132	20.066	-0.009 ± 0.008	-0.037 ± 0.006
SXDSPM J021702.0-052310	34.25844	-5.38629	21.361	20.552	19.495	18.638	-0.014 ± 0.004	-0.045 ± 0.006
SXDSPM J021705.9-053140	34.27470	-5.52778	20.960	20.232	19.390	18.657	0.054 ± 0.006	0.002 ± 0.002
SXDSPM J021706.2-052737	34.27605	-5.46043	22.959	22.283	21.704	21.334	0.026 ± 0.002	-0.000 ± 0.002
SXDSPM J021706.6-052724	34.27770	-5.45692	19.473	19.491	19.593	19.467	0.090 ± 0.002	0.018 ± 0.006
SXDSPM J021707.2-052427	34.28022	-5.40771	22.629	21.713	19.924	18.797	-0.010 ± 0.006	-0.027 ± 0.002
SXDSPM J021708.0-051419	34.28370	-5.23883	21.888	21.224	20.844	20.512	0.025 ± 0.002	-0.009 ± 0.004
SXDSPM J021708.6-052501	34.28613	-5.41700	21.210	20.640	20.340	20.056	0.021 ± 0.002	-0.039 ± 0.006
SXDSPM J021709.9-052437	34.29164	-5.41042	19.359	18.949	18.765	18.121	0.006 ± 0.010	-0.048 ± 0.004
SXDSPM J021712.5-052133	34.30238	-5.35927	25.035	23.881	22.015	21.002	-0.016 ± 0.004	-0.021 ± 0.002
SXDSPM J021719.9-052038	34.33308	-5.34394	23.456	22.977	21.860	21.242	0.018 ± 0.002	-0.014 ± 0.002
SXDSPM J021720.9-053642	34.33718	-5.61191	22.624	22.024	21.111	20.589	0.038 ± 0.004	-0.012 ± 0.002
SXDSPM J021722.4-053136	34.34335	-5.52691	25.028	23.684	21.769	20.732	0.036 ± 0.006	0.017 ± 0.004
SXDSPM J021730.6-052459	34.37758	-5.41639	19.645	19.246	19.093	18.484	0.041 ± 0.006	-0.029 ± 0.012
SXDSPM J021732.2-053558	34.38418	-5.59953	20.670	20.113	19.875	19.462	0.001 ± 0.006	-0.036 ± 0.004
SXDSPM J021734.8-051850	34.39506	-5.31412	21.303	20.604	19.945	19.372	-0.007 ± 0.004	-0.035 ± 0.004
SXDSPM J021736.1-053647	34.40074	-5.61307	22.646	22.264	22.066	21.865	0.058 ± 0.004	0.016 ± 0.006
SXDSPM J021744.6-052116	34.43611	-5.35462	20.260	19.765	19.535	19.017	0.027 ± 0.002	-0.011 ± 0.006
SXDSPM J021745.3-053035	34.43904	-5.50984	21.983	21.348	20.487	19.975	0.020 ± 0.002	-0.012 ± 0.002
SXDSPM J021756.5-053530	34.48554	-5.59187	22.863	22.261	21.071	20.434	0.092 ± 0.002	-0.052 ± 0.002
SXDSPM J021758.2-052304	34.49284	-5.38466	24.030	23.477	22.989	22.585	0.019 ± 0.002	-0.008 ± 0.004
SXDSPM J021805.6-053254	34.52353	-5.54855	20.584	19.971	19.668	19.177	0.046 ± 0.004	-0.024 ± 0.006
SXDSPM J021806.6-053612	34.52764	-5.60350	22.747	22.552	22.428	22.232	-0.017 ± 0.004	-0.041 ± 0.006
SXDSPM J021806.8-053613	34.52869	-5.60379	22.519	21.738	20.187	19.262	-0.019 ± 0.006	-0.044 ± 0.004
SXDSPM J021809.7-052547	34.54078	-5.42992	24.105	23.070	21.488	20.653	0.032 ± 0.002	0.013 ± 0.008
SXDSPM J021818.2-052739	34.57622	-5.46110	20.333	19.746	19.515	19.002	0.007 ± 0.004	-0.050 ± 0.006
SXDSPM J021819.0-052129	34.57918	-5.35825	21.402	20.613	19.516	18.610	0.027 ± 0.004	-0.024 ± 0.004
SXDSPM J021830.8-051918	34.62859	-5.32185	23.006	22.375	21.998	21.704	0.002 ± 0.002	-0.023 ± 0.002
SXDSPM J021833.5-052918	34.63963	-5.48858	22.841	21.973	20.409	19.523	0.056 ± 0.004	-0.037 ± 0.004
SXDSPM J021835.5-051734	34.64794	-5.29294	22.605	21.889	21.000	20.489	0.001 ± 0.002	-0.063 ± 0.004
SXDSPM J021840.0-053623	34.66670	-5.60661	≥ 27.3	26.085	24.381	22.618	0.184 ± 0.024	0.024 ± 0.028
SXDSPM J021850.4-053200	34.71003	-5.53342	20.818	20.126	19.467	18.740	0.023 ± 0.010	-0.041 ± 0.004
SXDSPM J021856.8-044522	34.73684	-4.75612	22.112	21.248	19.816	19.002	0.020 ± 0.002	-0.025 ± 0.008
SXDSPM J021858.4-052439	34.74341	-5.41092	21.530	20.574	19.157	18.121	0.075 ± 0.004	0.040 ± 0.018
SXDSPM J021901.2-051403	34.75517	-5.23426	24.560	23.221	21.297	20.255	0.049 ± 0.006	-0.011 ± 0.004
SXDSPM J021902.7-053628	34.76158	-5.60784	20.670	19.851	18.860	18.082	-0.035 ± 0.012	-0.044 ± 0.004
SXDSPM J021903.0-053131	34.76257	-5.52552	20.963	20.194	19.293	18.482	-0.022 ± 0.004	-0.033 ± 0.002
SXDSPM J021903.7-052540	34.76557	-5.42783	22.867	22.167	20.903	20.143	0.011 ± 0.004	-0.019 ± 0.002
SXDSPM J021908.5-053002	34.78549	-5.50076	21.144	20.406	19.500	18.737	0.063 ± 0.002	-0.056 ± 0.006
SXDSPM J021911.0-045902	34.79612	-4.98411	21.049	21.244	21.398	21.520	-0.015 ± 0.006	-0.091 ± 0.002
SXDSPM J021914.8-045312	34.81205	-4.88669	22.594	21.743	20.394	19.608	0.023 ± 0.002	-0.001 ± 0.002
SXDSPM J021914.8-050120	34.81208	-5.02240	23.248	22.601	21.223	20.488	0.027 ± 0.002	-0.015 ± 0.002
SXDSPM J021918.6-045833	34.82772	-4.97598	23.953	23.643	23.461	23.240	0.041 ± 0.004	0.009 ± 0.010
SXDSPM J021925.1-051610	34.85480	-5.26966	24.550	23.320	21.791	20.888	0.023 ± 0.002	-0.008 ± 0.008
SXDSPM J021925.7-050051	34.85742	-5.01442	19.927	19.363	19.074	18.511	0.019 ± 0.008	-0.075 ± 0.010
SXDSPM J021929.2-045819	34.87201	-4.97220	23.146	22.281	20.512	19.556	0.061 ± 0.006	0.035 ± 0.006
SXDSPM J021935.5-050422	34.89807	-5.07289	22.303	21.430	20.061	19.267	-0.007 ± 0.004	-0.035 ± 0.004
SXDSPM J021936.0-051658	34.90005	-5.28305	20.373	19.878	19.695	19.378	0.006 ± 0.004	-0.018 ± 0.002
SXDSPM J021936.2-050341	34.90105	-5.06145	20.809	20.271	19.828	19.473	0.067 ± 0.008	0.010 ± 0.006
SXDSPM J021938.6-045727	34.91113	-4.95770	25.630	23.841	21.845	20.383	0.076 ± 0.010	-0.020 ± 0.004
SXDSPM J021939.9-045216	34.91662	-4.87112	22.535	21.806	20.811	20.262	0.023 ± 0.002	-0.018 ± 0.004
SXDSPM J021942.3-044706	34.92665	-4.78525	23.566	22.894	22.229	21.844	-0.009 ± 0.008	-0.045 ± 0.004
SXDSPM J021943.9-044432	34.93307	-4.74238	22.059	21.078	19.541	18.541	0.017 ± 0.002	-0.054 ± 0.008
SXDSPM J021952.2-045056	34.96781	-4.84908	21.380	20.357	19.436	18.679	0.012 ± 0.002	-0.042 ± 0.006

Table 3. (Continued.)

SXDSPM J021953.9-051649	34.97485	-5.28045	22.290	21.608	20.948	20.537	0.074 ± 0.004	-0.022 ± 0.008
SXDSPM J021958.4-044516	34.99338	-4.75447	20.862	20.156	19.558	19.020	0.030 ± 0.004	-0.021 ± 0.002
SXDSPM J022001.8-045640	35.00766	-4.94449	21.073	20.326	19.478	18.785	0.014 ± 0.008	-0.029 ± 0.002
SXDSPM J022005.0-045022	35.02086	-4.83953	20.564	19.919	19.653	19.230	0.002 ± 0.002	-0.069 ± 0.004
SXDSPM J022008.8-050351	35.03694	-5.06436	22.370	21.614	20.343	19.619	0.041 ± 0.006	-0.011 ± 0.002
SXDSPM J022009.5-050912	35.03992	-5.15360	22.600	21.935	21.072	20.589	0.004 ± 0.004	-0.029 ± 0.004
SXDSPM J022010.3-050259	35.04295	-5.04978	25.174	24.962	24.666	24.316	0.088 ± 0.014	-0.023 ± 0.018
SXDSPM J022013.1-045912	35.05474	-4.98686	21.256	20.525	19.642	18.973	0.020 ± 0.002	-0.021 ± 0.004
SXDSPM J022013.7-051353	35.05711	-5.23166	24.690	23.278	21.038	19.823	0.067 ± 0.006	0.003 ± 0.006
SXDSPM J022017.4-051313	35.07290	-5.22034	23.826	23.254	22.519	22.072	-0.000 ± 0.002	-0.034 ± 0.004
SXDSPM J022024.0-050606	35.10031	-5.10171	22.865	22.476	22.198	21.979	0.041 ± 0.010	-0.084 ± 0.004
SXDSPM J022025.7-051028	35.10718	-5.17455	22.754	21.994	20.646	19.921	0.016 ± 0.004	-0.030 ± 0.002
SXDSPM J022032.5-050834	35.13545	-5.14289	22.599	21.864	20.859	20.311	0.021 ± 0.002	0.004 ± 0.004

* Equinox J2000, epoch 2003.67.

** Corrected isophotal magnitudes from catalogs of Furusawa et al. (2008).

† Proper motions in arcseconds per year.